International Journal of Solids and Structures 51 (2014) 2529–2538

Contents lists available at ScienceDirect

International Journal of Solids and Structures

journal homepage: www.elsevier.com/locate/ijsolstr

Transverse conductivity and longitudinal shear of elliptic fiber composite with imperfect interface

V.I. Kushch *, V.S. Chernobai

Institute for Superhard Materials of the National Academy of Sciences, 04074 Kiev, Ukraine

ARTICLE INFO

Article history:
Received 28 December 2013
Received in revised form 20 February 2014
Available online 28 March 2014

Keywords:
Composite
Ellipse
Imperfect interface
Effective conductivity
Multipole expansion
Unit cell model

ABSTRACT

The paper addresses the problem of calculating the local fields and effective transport properties and longitudinal shear stiffness of elliptic fiber composite with imperfect interface. The Rayleigh type representative unit cell approach has been used. The micro geometry of composite is modeled by a periodic structure with a unit cell containing multiple elliptic inclusions. The developed method combines the superposition principle, the technique of complex potentials and certain new results in the theory of special functions. An appropriate choice of the potentials provides reducing the boundary-value problem to an ordinary, well-posed set of linear algebraic equations. The exact finite form expression of the effective stiffness tensor has been obtained by analytical averaging the local gradient and flux fields. The convergence of solution has been verified and the parametric study of the model has been performed. The obtained accurate, statistically meaningful results illustrate a substantial effect of imperfect interface on the effective behavior of composite.

1. Introduction

The interfaces play an important, often dominant role in determining the local and overall behavior of heterogeneous solids. The "perfect interface bonding" (more correctly, perfect thermal/mechanical contact) assumption widely used in micromechanics is merely a more or less appropriate idealization. In fact, the interfaces are *always* imperfect: the atomic lattices mismatch, poor mechanical or chemical adherence, surface contamination, oxide and interphase diffusion/reaction layers, coatings, interface debonding or cracking, etc. are possible reasons of imperfectness. Even in the case of ideal contact between the constituents, the interface resistance due to interfacial phonon scattering makes the composite properties size-dependent (e.g., Every et al., 1992). Nanocomposites (see, e.g., Luo and Wang, 2009 and the references therein) give an another example of the size dependence due to interface effects.

In this paper, we focus on the two-dimensional (2D) scalar (conductivity and out-of-plane shear) models of matrix type composites. The problems involving composites of circular inclusions with imperfect interface have received a considerable attention in the literature. Probably, the most known is the work by Hasselman and Johnson (1987) which extends the famous Maxwell's formula for effective conductivity to a fibrous composite with imperfect interface. An effect of interfacial characteristics on the effective thermal conductivity of isotropic two-dimensional periodic (square or hexagonal) composites of circular cylinders is studied by Lu and Lin (1995). An approximate solution for a random composite of imperfectly bonded fibers (Lu and Song, 1996) takes into account pair wise fiber-to-fiber interactions and radial distribution function. Graham and McDowell (2003) estimated thermal conductivity of random fiber composite with imperfect interface by the finite element analysis of the many-inclusion cell model. These and other similar (Achenbach and Zhu, 1989; Hashin, 1990; Gao, 1995 among others) works are based on the assumption that flux/traction is continuous whereas temperature/displacement is discontinuous across the interface. Specifically, a jump in the displacement is proportional, in terms of "spring-factor-type" interface parameters, to the interface traction. When these interface parameters uniform along the entire length of the material interface, the model is said to represent a *homogeneously* imperfect interface. The case of *inhomogeneous* interface in out-of-plane shear was considered by Ru and Schiavone (1997).

In the real-life composites, we do not expect the inclusions to be of exact canonical shape. The above mentioned models are adequate for the heterogeneous solids with equiaxial inclusions where the mean radius is the only length parameter of inclusion. When the inclusion's shape deviates considerably from the circular one, we need an additional length parameter to quantify it. In this case, an ellipse (also possessing two length parameters) appears to be

* Corresponding author. Tel./fax: +380 444329544.
E-mail address: vkushch@bigmir.net (V.I. Kushch).

http://dx.doi.org/10.1016/j.ijsolstr.2014.03.024
0020-7683/

more appropriate model shape. In particular, an infinitely thin elliptic hole is a convenient model of the straight crack. Therefore, the "solid with elliptic inclusions" model seems appealing in both theoretical and practical aspects.

The solution for a single elliptic inclusion is well known (see, e.g., Ru and Schiavone, 1996, and the references therein). At the same time, the analytical solutions for the interacting elliptic inclusions are limited to a few. A certain progress is observed in the conductivity problem where the multipole expansion solution has been obtained for the finite (Yardley et al., 1999) and periodic (Yardley et al., 2001; Kuo, 2010) arrays of elliptical cylinders. The complete solutions for a finite array of elliptic inclusions in the plane (Kushch et al., 2005) and half-plane (Kushch et al., 2006) have been obtained by combining the multipole expansion approach with the Kolosov–Muskhelishvili's technique of complex potentials. This approach has been further developed and applied to evaluation of the stress intensity factors (Kushch et al., 2009a) and effective stiffness (Kushch et al., 2009b) of cracked solids. The theory of the multipole expansion method in application to the solids with elliptic inclusions is given in the book by Kushch (2013). Among the available numerical studies on effective conductivity of fiber composites, we mention the work by Lu (1994) who applied the boundary collocation scheme for evaluating effective conductivity of the rectangular arrays of elliptic inclusions. Byström (2003) studied the many-particle cell model for the periodic and random structure composites with circular or elliptic inclusions by the finite element method.

To our best knowledge, the elliptic fiber composites with imperfect interface never been addressed in the micromechanics literature. The paper by Shen et al. (2000) who considered a single elliptic inclusion with homogeneously imperfect interface is probably the only effort in this direction. The aim of our work is to close this gap by developing the micromechanical model of elliptic fiber composite for the conductivity and out-of-plane shear problems, able to take into account microstructure of composite and interactions between the inclusions with imperfect bonding to the matrix.

The outline of this paper is as follows. First, we formulate the problem in terms of complex potentials. Second, a general solution of the problem for a single, imperfectly bonded elliptic inclusion in the inhomogeneous far field is derived and tested numerically. Next, we incorporate this solution into a general scheme of the multipole expansion method to get a complete solution for a representative unit cell (RUC) model of elliptic fiber composite with imperfect interface. By analytical averaging the local gradient and flux fields, the exact finite form expression of the effective conductivity tensor has been obtained. The effect of interface conductivity on the effective behavior of composite has been evaluated. The background theory is provided in Appendices.

2. Governing equations in terms of complex variables

We consider a steady heat conduction in the unidirectional elliptic fiber composite due to transverse heat flux. In this case, the two-dimensional (2D) model is adequate to study the phenomenon. We assume both the matrix and fibers to be isotropic. The governing equation is $\nabla\cdot\mathbf{q}=0$, where $\mathbf{q}=-\lambda\nabla T$ is the heat flux vector. Also, λ is the thermal conductivity, T and ∇T is the temperature and its gradient, respectively. In the case of constant λ, T obeys Laplace equation $\nabla^2 T=0$.

Our analysis employs the technique of complex potentials (e.g., Muskhelishvili, 1953). In terms of the complex variable $z=x_1+\mathrm{i}x_2$ representing the position vector $\mathbf{x}=(x_1,x_2)^T$ in Ox_1x_2 plane, Laplace equation reduces to

$$\nabla^2 T=\frac{\partial^2 T}{\partial z\partial\bar{z}}=0.$$

The temperature T and complex heat flux $q=q_1+\mathrm{i}q_2$ are expressed in terms of the complex potential $\varphi(z)$ as

$$T=\mathrm{Re}\varphi(z);\quad q=q_1+\mathrm{i}q_2=-\lambda\overline{\varphi'(z)}. \tag{1}$$

Here and below, prime denotes differentiation with respect to the whole argument and over-bar denotes the complex conjugate.

The mathematically equivalent mechanical problem in the 2D elasticity theory is out-of-plane shear, where u_3 is the only non-zero component of displacement vector $\mathbf{u}$:

$$u_1=u_2=0;\quad u_3=w(x_1,x_2).$$

In this case, two non-zero components of the stress tensor are σ_{13} and σ_{23}. The stress equilibrium equation $\nabla\cdot\sigma=0$ takes the form

$$\frac{\partial\sigma_{13}}{\partial x_1}+\frac{\partial\sigma_{23}}{\partial x_2}=0; \tag{2}$$

the Hooke's law reduces to

$$\sigma_{i3}=2\mu\varepsilon_{i3}=\mu\partial w/\partial x_i,\quad i=1,2. \tag{3}$$

It follows from Eqs. (2) and (3) that $\nabla^2 w=0$ whereas the strain compatibility condition

$$\frac{\partial\varepsilon_{13}}{\partial x_2}=\frac{\partial\varepsilon_{23}}{\partial x_1}=\frac{1}{2}\frac{\partial^2 w}{\partial x_1\partial x_2}$$

is obeyed identically. This problem is readily reformulated in terms of the complex potentials (Muskhelishvili, 1953). For $w=\mathrm{Re}\varphi(z)$, Eq. (3) takes the form analogous to Eq. (1): namely, the complex stress $\sigma=\sigma_{13}+\mathrm{i}\sigma_{23}=\mu\overline{\varphi'(z)}$. Hence, the conductivity problem we consider below can be also interpreted in the mechanical context as the out-of-plane shear of elastic fibrous composite, with replace T to w, $(-\lambda)$ to μ and q to σ.

3. Single inclusion in an inhomogeneous far field

3.1. The problem statement

Consider an unbounded plane, or matrix, containing a single elliptic inclusion. All the matrix- and inclusion-related quantities are indexed by "0" and "1", respectively: $T=T^{(0)}$ and $\lambda=\lambda_0$ in the matrix, $T=T^{(1)}$ and $\lambda=\lambda_1$ in the inclusion. To describe geometry of the problem, we introduce the Cartesian coordinate frame Ox_1x_2 so that its origin coincides with the centroid of ellipse whereas the Ox_1 and Ox_2 axes are directed along the major and minor axes of the ellipse. An aspect ratio of the ellipse is $e=l_2/l_1$, where l_1 and l_2 are the major and minor, respectively, semi-axes of the ellipse; its area $S_1=\pi l_1 l_2$. Another derivative geometric parameter to be used in our analysis is the inter-foci distance $2d$, where $d=\sqrt{l_1^2-l_2^2}$.

Alongside with conventional complex variable $z=x_1+\mathrm{i}x_2$, we will use the "elliptic" complex variable $\xi=\zeta+\mathrm{i}\eta$ introduced (e.g., Sneddon and Berry, 1958) as

$$z=d\cosh\xi=\frac{d}{2}(\upsilon+\upsilon^{-1}),\quad \upsilon=\exp\xi. \tag{4}$$

In fact, Eq. (4) defines an elliptic coordinate frame with ζ and η as "radial" and "angular" coordinates, respectively. In particular, the coordinate curve $\zeta=\zeta_0$ specified by the condition

$$\zeta_0=\ln\left(\frac{l_1+l_2}{d}\right)=\frac{1}{2}\ln\left(\frac{1+e}{1-e}\right) \tag{5}$$

coincides with the boundary of elliptic inclusion. Also, we denote $\upsilon_0=\exp\zeta_0$. It is important that at this boundary the functions $\upsilon^k=\upsilon_0^k\exp\mathrm{i}k\eta$ depend only on the angular coordinate η. This fact makes the complex variable ξ particularly useful for the domains

with elliptic boundaries. In the limiting case of circular ($e = 1$) inclusion, $d \to 0$, $\upsilon_0 \to \infty$, $\upsilon_0 d \to 2R$, $\eta \to \theta$ and $\upsilon d \to 2r\exp i\theta = 2z$ where r and θ are the circular coordinates. Another limiting case is an infinitely thin ($e = 0$) inclusion or slit/crack where $d = l_1$ and $\upsilon_0 = 1$.

The imperfect contact thermal between the matrix and inclusion is assumed in the form (Hasselman and Johnson, 1987):

$$h_c[\![T]\!]_L = q_n; \quad [\![q_n]\!]_L = 0, \tag{6}$$

where $q_n = -\lambda\nabla T\cdot\mathbf{n} = -\lambda\partial T/\partial n$ is the normal flux and $[\![f]\!]_L = (f^{(0)} - f^{(1)})|_L$ means a jump of quantity f across the interface $L : \zeta = \zeta_0$. The temperature field in and outside the inclusion is defined by the far temperature field T_{far}: from the physical consideration, $T^{(0)} \to T_{far}$ when $z \to \infty$. And, to complete the problem formulation, we impose $T^{(1)}(0) = 0$. Our goal is to determine temperature in and outside the inclusion.

3.2. Formal solution

The temperature $T^{(1)}$ is written in terms of the complex potential φ_1 as

$$T^{(1)} = \mathrm{Re}\varphi_1, \quad \varphi_1 = \sum_k D_k\upsilon^{-k}, \tag{7}$$

where $D_k = D_{-k}$ (e.g., Muskhelishvili, 1953) due to the fact that $T^{(1)}$ is finite everywhere in the inclusion ($z \in S_1$). Taking $T^{(1)}(0) = 0$ into account yields

$$\varphi_1 = \sum_{k=1}^{\infty} D_k\left(\upsilon^k + \upsilon^{-k}\right). \tag{8}$$

The same reasonings apply to the far temperature field T_{far} assumed to be regular in a vicinity of inclusion, so

$$T_{far} = \mathrm{Re}\varphi_{far}, \quad \varphi_{far} = \sum_{k=1}^{\infty} a_k\left(\upsilon^k + \upsilon^{-k}\right). \tag{9}$$

An important particular case is the constant far heat flux $Q_{far} = -\lambda_0 G$, where $G = G_1 + iG_2$. The corresponding temperature $T_{far} = G_1x_1 + G_2x_2 = \mathrm{Re}\left(\overline{G}z\right)$. From here, $a_k = \delta_{k1}d\overline{G}/2$, where δ_{ij} is the Kronecker delta.

The total temperature in the matrix $T^{(0)} = T_{far} + T_s$, where T_s is a disturbance due to the inclusion:

$$T^{(0)} = \mathrm{Re}\varphi_0, \quad \varphi_0 = \varphi_{far} + \varphi_s. \tag{10}$$

Its asymptotic behavior ($T_s \to 0$ with $z \to \infty$) implies that φ_s series expansion involves only negative powers of υ, i.e.,

$$\varphi_s = \sum_{k=1}^{\infty} A_k\upsilon^{-k}. \tag{11}$$

In what follows, however, we will conveniently write

$$\varphi_0 = \sum_k (A_k + a_k)\upsilon^{-k}, \tag{12}$$

where $A_k \equiv 0$ for $k \leqslant 0$ and $a_k = a_{-k}$.

3.3. Resolving set of equations

The normal flux continuity condition $[\![q_n]\!]_L = 0$ is equivalent to $\mathrm{Im}[\![\lambda\varphi(z)]\!]_L = 0$ (e.g., Muskhelishvili, 1953), so instead of the second condition in Eq. (6) we use

$$\widetilde{\lambda}_1(\varphi_1 - \overline{\varphi_1}) = \varphi_0 - \overline{\varphi_0}, \tag{13}$$

where $\widetilde{\lambda}_1 = \lambda_1/\lambda_0$. At the interface L, $\upsilon = \upsilon_0 t$, where $t = \exp i\eta$; hence, $\overline{\upsilon} = \upsilon_0 t^{-1}$. By substituting φ_1 of Eq. (8) and φ_0 of Eq. (12) into Eq. (13), we get

$$\widetilde{\lambda}_1\left(\sum_k D_k\upsilon_0^{-k}t^{-k} - \sum_k \overline{D_k}\upsilon_0^k t^{-k}\right) = \sum_k (A_k + a_k)\upsilon_0^{-k}t^{-k} - \sum_k\left(\overline{A_{-k}} + \overline{a_k}\right)\upsilon_0^k t^{-k}.$$

In view of the orthogonality property of Fourier harmonics $t^k = \exp ik\eta$, we come readily to a set of linear relations

$$\widetilde{\lambda}_1\left(D_k\upsilon_0^{-k} - \overline{D_k}\upsilon_0^k\right) = (A_k + a_k)\upsilon_0^{-k} - \overline{a_k}\upsilon_0^k \tag{14}$$

for $k > 0$.

Our objective is to find the multipole expansion coefficients A_k. To this end, we take the first interface condition of Eq. (6)

$$h_c(T_0 - T_1) = -\lambda_0\frac{\partial T_0}{\partial n}$$

in terms of potentials as

$$\varphi_0 + \overline{\varphi_0} = \varphi_1 + \overline{\varphi_1} - \frac{\lambda_0}{h_c}\left(\frac{\partial\varphi_0}{\partial n} + \overline{\frac{\partial\varphi_0}{\partial n}}\right).$$

At the elliptic interface $\zeta = \zeta_0$,

$$\frac{\partial\varphi}{\partial n} = \frac{1}{d\sqrt{\sinh^2\zeta_0 + \sin^2\eta}}\frac{\partial\varphi}{\partial\zeta}.$$

So we get

$$\widetilde{\lambda}_1(\varphi_0 + \overline{\varphi_0}) = \widetilde{\lambda}_1(\varphi_1 + \overline{\varphi_1}) + \beta\left(\frac{\partial\varphi_0}{\partial\zeta} + \overline{\frac{\partial\varphi_0}{\partial\zeta}}\right), \tag{15}$$

where

$$\beta = -\frac{\lambda_1}{h_c l_2}\frac{1}{\sqrt{1 + \alpha\sin^2\eta}}, \tag{16}$$

$\alpha = \sinh^{-2}\zeta_0$ and $l_2 = d\sinh\zeta_0$ is the minor semi-axis of elliptic inclusion.

Remark 1. By contrast to the perfect interface ($h_c = \infty$) case, for a finite h_c a "size effect" is observed, i.e., the obtained results are dependent on the inclusion size (e.g., Benveniste and Miloh, 1986). This is a direct consequence of the first interface condition of Eq. (13): h_c dimensionality is (Wt/m^{2}K). The dimensionless complex $h_c l_2/\lambda_1$ entering Eq. (16) can be viewed (e.g., Lu and Lin, 1995) as the interface Biot number/criterion.

Combination of Eq. (15) with Eq. (13) yields

$$\left(\widetilde{\lambda}_1 + 1\right)\varphi_0 + \left(\widetilde{\lambda}_1 - 1\right)\overline{\varphi_0} = 2\widetilde{\lambda}_1\varphi_1 + \beta\left(\frac{\partial\varphi_0}{\partial\zeta} + \overline{\frac{\partial\varphi_0}{\partial\zeta}}\right).$$

In view of Eq. (12) and the remarkable property $\partial\upsilon/\partial\zeta = \upsilon$, one finds that

$$\left(\widetilde{\lambda}_1 + 1\right)\sum_n (A_n + a_n)\upsilon^{-n} + \left(\widetilde{\lambda}_1 - 1\right)\sum_n\left(\overline{A_n} + \overline{a_n}\right)\overline{\upsilon^{-n}} = 2\widetilde{\lambda}_1\sum_n D_n\upsilon^{-n} - \beta\left(\sum_n n(A_n + a_n)\upsilon^{-n} + \sum_n n\left(\overline{A_n} + \overline{a_n}\right)\overline{\upsilon^{-n}}\right).$$

Now, we multiply by t^k: $k = 1, 2, \ldots$ and integrate over a period $0 \leqslant \eta \leqslant 2\pi$ to get another infinite set of linear equations:

$$\left(\widetilde{\lambda}_1 + 1\right)(A_k + a_k)\upsilon_0^{-k} + \left(\widetilde{\lambda}_1 - 1\right)\overline{a_{-k}}\upsilon_0^k = 2\widetilde{\lambda}_1 D_k\upsilon_0^{-k} - \sum_n n(A_n + a_n)\upsilon_0^{-n}\beta_{k-n} - \sum_n n\left(\overline{A_n} + \overline{a_n}\right)\upsilon_0^{-n}\beta_{k+n}, \tag{17}$$

where

$$\beta_k = \beta_{-k} = \frac{1}{2\pi}\int_L \beta t^k dt = -\frac{1}{2\pi}\frac{\lambda_1}{h_c l_2}\int_0^{2\pi}\frac{\exp(ik\eta)}{\sqrt{1+\alpha\sin^2\eta}}d\eta. \quad (18)$$

For the recurrent procedure of β_k evaluation, see Appendix A.

The last step is removing the D_k. We express them from Eq. (14) as

$$\widetilde{\lambda}_1 D_k = \frac{A_k \upsilon_0^{-2k}}{(\upsilon_0^{-2k}-\upsilon_0^{2k})} + \frac{\overline{A_k}}{(\upsilon_0^{-2k}-\upsilon_0^{2k})} + a_k \quad (19)$$

and substitute into Eq. (17) to get the final form of the linear system:

$$\left(\widetilde{\lambda}_1+1\right)A_k - 2\frac{A_k\upsilon_0^{-2k}}{(\upsilon_0^{-2k}-\upsilon_0^{2k})} - 2\frac{\overline{A_k}}{(\upsilon_0^{-2k}-\upsilon_0^{2k})} + \left(\widetilde{\lambda}_1-1\right)\left(a_k+\overline{a_k}\upsilon_0^{2k}\right)$$
$$+\sum_{n=1}^{\infty} n\upsilon_0^{k-n}\left(A_n\beta_{k-n}+\overline{A_n}\beta_{k+n}\right)+\sum_n n\upsilon_0^{k-n}\left(a_n\beta_{k-n}+\overline{a_n}\beta_{k+n}\right)=0;$$
$$k=1,2,\ldots. \quad (20)$$

We mention three degenerate cases of the considered problem, they are (a) perfect interface $h_c=\infty$, (b) non-conducting interface $h_c=0$ and (c) circular inclusion, where the solution is elementary (Kushch, 2013, e.g.,) and, in the case of uniform far flux, the dipole moment A_1 is the only non-zero expansion coefficient in Eq. (11). A complete solution for a finite h_c is given by the infinite series of Eqs. (12) and (8) and hence requires an infinite set of linear equations of Eq. (20) to be solved.

Remark 2. The above solution procedure applies equally to the more general case of *inhomogeneously* imperfect interface: $h_c = h_c(\eta)$. The only difference consists in numerical evaluation of the integrals $\beta_k = \frac{1}{2\pi}\int_L \beta t^k dt$. The only exception is $h_c(\eta) = K\sqrt{1+\alpha\sin^2\eta}$ (K being a constant) where $\beta_k = 0$ for all $k \neq 0$ which makes the solution elementary. It can be readily shown that this solution corresponds to the case of a thin interphase layer between the inclusion and matrix, with confocal inner and outer boundary.

3.4. Numerical example

An approximate numerical solution of Eq. (20) up to arbitrary accuracy ε can be found by the truncation method (Kantorovich and Krylov, 1964) which implies retaining a finite number $n_{\max}(\varepsilon)$ of harmonics in Eq. (11) and the same number of equations in the linear system of Eq. (20). An approximate solution obtained this way tends to exact one as $n_{\max}\to\infty$. In so doing, it is important to keep in mind that convergence rate is substantially affected by the problem parameters. As expected, convergence accelerates when we approach the degenerate cases, i.e., for (a) $h_c\to\infty$, (b) $h_c\to 0$ and (c) $e=1$ and arbitrary h_c.

For any finite h_c, $n_{\max}$ increases when $e\to 0$: to maintain an error in the numerical calculations of order 1%, Shen et al. (2000) recommended $n_{\max}=3$ for $1>e>1/3$, $n_{\max}=5$ for $1/3>e>1/6$ and $n_{\max}=7$ for $1/6>e>1/9$. The data in Table 1 demonstrate convergence of A_1 in terms of the number of harmonics, $n_{\max}$ for inclusion with $e=0.1$ and $\widetilde{\lambda}_1=\lambda_1/\lambda_0=1000$. Also, in this and all subsequent numerical tests we operate with the normalized interface conductivity coefficient $\widetilde{h}_c = h_c l_1/\lambda_0$. The far field is given by temperature gradient $G=1$ (flux in x_1 direction). As seen from the table, $n_{\max}=20$ provides 5-digit accuracy of A_1 and related parameters.

Table 1
Convergence of A_1 in terms of the number of harmonics, $n_{\max}$ for the temperature gradient $G=1$, aspect ratio $e=0.1$ and inclusion-to-matrix conductivity ratio $\widetilde{\lambda}_1=1000$.

$\widetilde{h}_c$	$n_{\max}$					
	1	3	5	10	15	20
∞	1.09350	1.09350	1.09350	1.09350	1.09350	1.09350
10^3	1.08941	1.08942	1.08943	1.08944	1.08944	1.08944
10^2	1.05377	1.05476	1.05539	1.05596	1.05617	1.05620
10	0.78718	0.82314	0.83327	0.83714	0.83763	0.83767
1	0.16234	0.24290	0.24971	0.25130	0.25148	0.25149
10^{-1}	−0.07627	−0.06041	−0.05949	−0.05927	−0.05925	−0.05924
10^{-2}	−0.10704	−0.10532	−0.10522	−0.10520	−0.10520	−0.10520
10^{-3}	−0.11020	−0.11003	−0.11002	−0.11002	−0.11002	−0.11002
0	−0.11055	−0.11055	−0.11055	−0.11055	−0.11055	−0.11055

It was mentioned already that, for a finite h_c, the flux in the inclusion is non-uniform even in the case of uniform far flux. The inclusion-averaged flux

$$\langle q_1\rangle_{S_1} = \frac{1}{S_1}\int_{S_1} q_1 ds = -\frac{2\lambda_1}{d}\mathrm{Re}D_1$$

is also affected by h_c. Fig. 1 shows an effect of h_c on the average flux $\langle q_1\rangle_{S_1}$ where $\widetilde{\lambda}_1$ is taken after (Shen et al., 2000): $\widetilde{\lambda}_1 = 30.17/1.02 \simeq 29.6$.

As seen from the plots, for $\widetilde{h}_c \leqslant 0.01$ and $\widetilde{h}_c \geqslant 100$ we approach two opposite degenerate cases, namely, those of pore and perfect interface regardless of the shape factor e. For large $\widetilde{h}_c$ values, however, $\langle q_1\rangle_{S_1}$ is greatly affected by this parameter and grows from $\langle q_1\rangle_{S_1}=1.94$ for $e=1.0$ to $\langle q_1\rangle_{S_1}=5.13$ for $e=0.2$. Noteworthy, the numerical data reported by Shen et al. (2000) are incorrect.

The straightforward application of the above theory to the micromechanics is to develop a single-inclusion based (dilute, Maxwell, self-consistent, differential, etc.) scheme for evaluation of the effective conductivity of elliptic fiber composite with imperfect interface. In what follows, we use it as the background theory for developing the advanced, RUC model of composite.

4. RUC model of composite

We consider the representative unit cell (RUC) model of composite with inclusions of elliptic shape. Specifically, we study a composite where the elliptic fibers form a periodic micro structure with the period a along the axes Ox_1 and Ox_2 of the global Cartesian

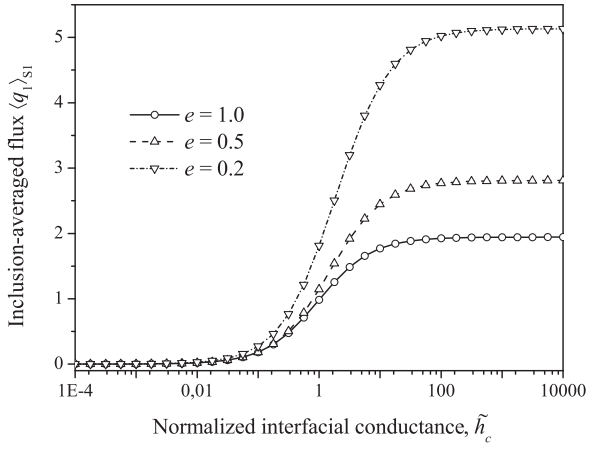

Fig. 1. The inclusion-averaged heat flux $\langle q_1\rangle_{S_1}$ as a function of normalized interface conductivity $\widetilde{h}_c$.

coordinate frame. The unit cell of this material is a square containing N inclusions. To minimize a number of parameters, we assume all the inclusions to be identical and equally oriented (in x_1 direction), see Fig. 2. Consideration of composite with inclusions of various size, shape, orientation and properties follows the same way. Within a cell, inclusions are located arbitrarily but without overlapping other inclusions of this and adjacent cells. At the same time, the inclusions can cross the cell boundary: we consider the inclusion as belonging to the cell if the center of inclusion lies inside it. Thus, geometry of the unit cell is defined by the side length a, the coordinates (X_{1q}, X_{2q}) of the center O_q of qth inclusion $(1 \leqslant q \leqslant N)$, their aspect ratio $e = l_2/l_1$ and inter foci length $2d$. The whole composite bulk is obtained by replicating the unit cell in two orthogonal directions. The volume content of inclusions $c = N\pi l_1 l_2/a^2$. The random RUC geometry shown in Fig. 2 is generated using the Monte Carlo procedure of Metropolis type (see, e.g., Byström, 2003 for the details).

Besides the global Cartesian coordinate frame Ox_1x_2, we introduce the inclusion-related local coordinate frames $O_qx_{1q}x_{2q}$ whose origins coincide with the center of q-th inclusion whereas the O_qx_{1q} and O_qx_{2q} axes are parallel to the corresponding axes of the global coordinate frame. The global $z = x_1 + \mathrm{i}x_2$ and local $z_q = x_{1q} + \mathrm{i}x_{2q}$ variables are related by $z = z_q + Z_q$ $(Z_q = X_{1q} + \mathrm{i}X_{2q})$. The local, inclusion-related elliptic coordinates $\xi_q = \zeta_q + \mathrm{i}\eta_q$ are defined by the formula analogous to Eq. (4):

$$z_q = d\cosh(\xi_q) = \frac{d}{2}(\upsilon_q + \upsilon_q^{-1}), \quad \upsilon_q = \exp\xi_q. \tag{21}$$

At the qth inclusion surface L_q, we have $\zeta_q = \zeta_0$ and $\upsilon_0 = \exp\zeta_0$.

The temperature gradient and flux fields are assumed *macroscopically uniform* and defined by the constant macroscopic gradient G. Due to the cell-type periodicity of geometry, the local temperature field is a quasi-periodic function of coordinates:

$$T(z + a) - T(z) = G_1 a; \quad T(z + \mathrm{i}a) - T(z) = G_2 a. \tag{22}$$

4.1. Analytical solution

We use the superposition principle to write a general solution of the out-of-plane problem as

$$T^{(0)} = \mathrm{Re}\,\widehat{\varphi}, \quad \widehat{\varphi} = \varphi_{far} + \sum_{p=1}^{N}\widehat{\varphi}^{(p)}, \tag{23}$$

where, as before, $\varphi_{far} = \overline{\Gamma}z$ is a linear term and

$$\widehat{\varphi}^{(p)} = \sum_{n=1}^{\infty}A_n^{(p)}\widehat{\upsilon}_n(z_p) \quad (1 \leqslant p \leqslant N). \tag{24}$$

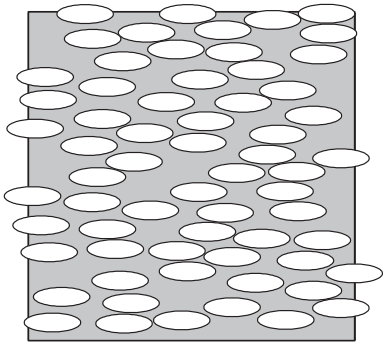

Fig. 2. RUC model of the random structure composite with elliptic fibers: number of inclusions per cell $N = 48$, aspect ratio $e = 1/3$, volume content of inclusions $c = 0.5$.

The functions $\widehat{\upsilon}_n$ in Eq. (24) are periodic complex potentials defined by Eq. (C.1) of Appendix C and $A_n^{(p)}$ are the complex series expansion coefficients to be found. The properties Eq. (C.4) of the functions $\widehat{\upsilon}_n$ enable fulfilling the periodicity conditions of Eq. (22). Substitution of Eqs. (23) and (24) into Eq. (22) gives us

$$\Gamma = G + \frac{\pi d\mathrm{i}}{a^2}\sum_{p=1}^{N}\mathrm{Im}A_1^{(p)}. \tag{25}$$

To fulfil the boundary conditions of Eq. (6), we first expand $\widehat{\varphi}$ in a vicinity of qth inclusion (in fact, with respect of its midpoint O_q) into the Laurent series of υ_q. Expansion of the linear term φ_{far} is elementary:

$$\varphi_{far} = \overline{\Gamma}Z_q + \frac{\overline{\Gamma}d}{2}(\upsilon_q + 1/\upsilon_q).$$

Expansion of the periodic disturbance terms $\widehat{\varphi}^{(p)}$, Eq. (24) employs Eq. (C.2) for the terms with $p = q$ and Eq. (C.5) for the rest of them. Omitting the algebra, we write

$$\widehat{\varphi} = \sum_k\left(A_k^{(q)} + a_k^{(q)}\right)(\upsilon_q)^{-k} \quad (A_k^{(q)} \equiv 0 \text{ for } k \leqslant 0), \tag{26}$$

where

$$a_k^{(q)} = \sum_{p=1}^{N}\sum_{n=1}^{\infty}A_n^{(p)}\eta_{nk}^{*pq} + \delta_{k,\pm1}\frac{\overline{\Gamma}d}{2} \tag{27}$$

and $\eta_{nk}^{*pq} = \eta_{nk}^{pq} + \widetilde{\eta}_{nk}^{pq}$. The explicit form of η_{nk}^{pq} and $\widetilde{\eta}_{nk}^{pq}$ is given by Eqs. (B.3) and (C.6), respectively. We note also that $a_k^{(q)}$ of Eq. (27) are the expansion coefficients of the regular part of solution and, hence, $a_{-k}^{(q)} = a_k^{(q)}$ is the necessary condition. For more details, see Kushch (2013).

The form of Eq. (26) is the same as of Eq. (12), so the only remaining step is substitution of Eq. (27) into Eq. (20) written for qth interface. After some algebra, we come to the following compact, convenient for numerical realization formulas:

$$\sum_{n=0}^{\infty}\left(A_n^{(q)}W_{nk}^{(1)} + \overline{A_n^{(q)}}W_{nk}^{(2)} + a_n^{(q)}v_{nk}^{(1)} + \overline{a_n^{(q)}}v_{nk}^{(2)}\right) = 0$$
$$q = 1, 2, \ldots, N; \quad k = 1, 2, \ldots; \tag{28}$$

where

$$W_{nk}^{(1)} = n\upsilon_0^{-n}\beta_{k-n} + \delta_{nk}\left[\left(\widetilde{\lambda}_1 + 1\right) - \frac{2\upsilon_0^{-2n}}{\upsilon_0^{-2n} - \upsilon_0^{2n}}\right]\upsilon_0^{-n};$$

$$W_{nk}^{(2)} = n\upsilon_0^{-n}\beta_{k+n} - \delta_{nk}\frac{2\upsilon_0^{-n}}{\upsilon_0^{-2n} - \upsilon_0^{2n}};$$

$$v_{nk}^{(1)} = n\upsilon_0^{-n}\beta_{k-n} - n\upsilon_0^{n}\beta_{k+n} + \delta_{nk}\left(\widetilde{\lambda}_1 - 1\right)\upsilon_0^{-n};$$

$$v_{nk}^{(2)} = n\upsilon_0^{-n}\beta_{k+n} - n\upsilon_0^{n}\beta_{k-n} + \delta_{nk}\left(\widetilde{\lambda}_1 - 1\right)\upsilon_0^{n}.$$

Numerical solution of the linear system Eq. (28) is obtained by the truncation method.

4.2. Effective conductivity tensor

The derived analytical solution provides evaluation of the local thermal fields in every point of the unit cell. For our purpose, it is important that these fields can be integrated analytically to obtain the exact, closed form formula for the effective transverse conductivity tensor $\Lambda^* = \left\{\lambda_{ij}^*\right\}$ of a fibrous composite defined by

$$\langle\mathbf{q}\rangle = -\Lambda^*\cdot\langle\nabla T\rangle, \tag{29}$$

where $\langle\nabla T\rangle$ and $\langle\mathbf{q}\rangle$ are the macroscopic temperature gradient and heat flux vector, respectively. In order to evaluate λ^*_{ij} for a given geometry and properties of composite, one has to conduct a series of numerical tests with various $\langle\nabla T\rangle$ and evaluate the macroscopic heat flux it causes. Specifically, $\lambda^*_{ij}=-\langle q_i\rangle$ for $\langle\nabla T\rangle=\mathbf{i}_j$, so we need an explicit expression of the macroscopic temperature gradient and heat flux corresponding to our temperature solution, Eqs. (23)–(28).

The macroscopic quantities $\langle\nabla T\rangle$ and $\langle\mathbf{q}\rangle$ are commonly defined as the volume-averaged values of the corresponding local fields:

$$\langle\nabla T\rangle\overset{def}{=}\frac{1}{V}\int_V\nabla T\mathrm{d}\mathbf{x};\quad \langle\mathbf{q}\rangle\overset{def}{=}\frac{1}{V}\int_V\mathbf{q}\mathrm{d}\mathbf{x}; \tag{30}$$

where V is a volume of the representative volume element (RVE) of composite. An alternate, surface averaging-based definition of the macroscopic conductivity parameters (Zuzovsky and Brenner, 1977):

$$\langle\nabla T\rangle\overset{def}{=}\frac{1}{V}\int_S T\mathbf{n}\mathrm{d}s,\quad \langle\mathbf{q}\rangle\overset{def}{=}\frac{1}{V}\int_S(\mathbf{q}\cdot\mathbf{n})\mathbf{x}\,\mathrm{d}s, \tag{31}$$

where S is a boundary of RVE, $\mathbf{x}=x_j\mathbf{i}_j$ is the position vector and $\mathbf{n}=n_j\mathbf{i}_j$ is the normal unit vector. The definition Eq. (31) is advantageous for the following reasons. First, it involves only the observable/measurable quantities – temperature and flux – at the surface of composite specimen. In essence, RVE is considered as a "black box" which makes the definition general, valid for composites with arbitrary interior microstructure. In context of our study, the most important is the fact that Eq. (31) holds true for composites with imperfect interfaces whereas volume averaging of Eq. (30) fails (Benveniste and Miloh, 1986). This is clearly seen from the Green formula-based identities

$$\frac{1}{V}\int_V\nabla T\mathrm{d}\mathbf{x}=\frac{1}{V}\int_S T\mathbf{n}\mathrm{d}s+\frac{1}{V}\sum_{i=1}^N\int_{S_i}[\![T]\!]\mathbf{n}\mathrm{d}s \tag{32}$$

and

$$\frac{1}{V}\int_V\mathbf{q}\mathrm{d}\mathbf{x}=\frac{1}{V}\int_S(\mathbf{q}\cdot\mathbf{n})\mathbf{x}\mathrm{d}s+\frac{1}{V}\sum_{i=1}^N\int_{S_i}[\![\mathbf{q}\cdot\mathbf{n}]\!]\mathbf{x}\mathrm{d}s. \tag{33}$$

where S_i is the ith interface and $[\![*]\!]$ means the function jump. The definitions Eqs. (30) and (31) coincide only in the case of continuous across the interface temperature T and normal flux $q_n=\mathbf{q}\cdot\mathbf{n}$. Eqs. (32) and (33) prove also that the average parameters defined by Eq. (2.20) of Cheng and Torquato (1997), Eq. (2.7) of Cheng and Torquato (1997) and by Eqs. (4.4) and (4.7) of Kuo (2013) are equivalent to Eq. (31). For more discussion on this subject, see Kushch and Sevostianov (2013) and Kushch (2013).

Due to macro periodicity of structure imposed by RUC model, the last one can serve as RVE of composite for the effective conductivity evaluation purpose. The general relations between the macroscopic parameters $\langle\nabla T\rangle$ and $\langle\mathbf{q}\rangle$ for the RUC model of composite (Kushch and Sevostianov, 2013) hold true for 2D. As would be expected from Eq. (22), $\langle\nabla T\rangle=G$. The formula for average heat flux in our case becomes

$$\langle\mathbf{q}\rangle=-\mathbf{\Lambda}_0\cdot\langle\nabla T\rangle+\frac{1}{a^2}\sum_{q=1}^N\mathbf{p}^{(q)}, \tag{34}$$

where

$$\mathbf{p}^{(q)}=\int_{L_q}\left[T^{(0)}q_n(\mathbf{x})-q_n\left(T^{(0)}\right)\mathbf{x}\right]\mathrm{d}L \tag{35}$$

and L_q is the qth matrix-inhomogeneity interface. In Eq. (35), integral is taken over the matrix side ($T=T^{(0)}$, $\mathbf{q}=\mathbf{q}^{(0)}$) of L_q; $q_n(T)=\mathbf{q}(T)\cdot\mathbf{n}$ is the normal flux and $q_n(\mathbf{x})=q_n(x_j)\mathbf{i}_j$. In the considered by us isotropic case, $q_n(\mathbf{x})=-\lambda_0\mathbf{n}$.

In the second term in Eq. (34), $\mathbf{p}^{(q)}$ is the induced dipole moment of qth inhomogeneity. For further discussion, see Kushch and Sevostianov (2013): here, we note only that the integrals in Eq. (35) involve only the matrix phase temperature field, $T^{(0)}$. Moreover, these integrals are identically zero for all but dipole term in the $T^{(0)}$ multipole expansion in a vicinity of inhomogeneity and represent contribution of these inhomogeneities to the overall conductivity tensor.

Evaluation of the integral of Eq. (35) over the elliptic boundary is ready. In complex variables, it takes the form

$$p^{(q)}=\lambda_0\int_{L_q}\left(\frac{\partial T^{(0)}}{\partial n}z-nT^{(0)}\right)\mathrm{d}L,$$

where $p^{(q)}=p_1^{(q)}+\mathrm{i}p_2^{(q)}$. In view of

$$z=d\cosh\xi,\quad \frac{\partial}{\partial n}=\frac{1}{d|\sinh\xi|}\frac{\partial}{\partial\zeta},\quad n=\frac{\sinh\xi}{|\sinh\xi|},\quad dL=d|\sinh\xi|d\eta,$$

Eq. (35) reduces to

$$p^{(q)}=\lambda_0\int_0^{2\pi}\left(\frac{\partial T^{(0)}}{\partial\xi_q}\cosh\xi_q-T^{(0)}\sinh\xi_q\right)\mathrm{d}\eta_q. \tag{36}$$

Recall that $T^{(0)}=\mathrm{Re}\,\widehat{\varphi}$; we substitute the local expansion of $\widehat{\varphi}$ given by Eq. (26) into Eq. (36). Only zero Fourier harmonics in η_q survives integration over the period, so we get

$$p^{(q)}=-\lambda_0\pi dA_1^{(q)}.$$

As would be expected, only the dipole term contributes to the effective conductivity of composite. Substitution of this expression into Eq. (34) gives the remarkably simple formula

$$-\frac{\langle q\rangle}{\lambda_0}=G+\frac{\pi d}{a^2}\sum_{q=1}^N A_1^{(q)}. \tag{37}$$

Together with Eqs. (29), re-written as

$$-\langle q\rangle=(\lambda^*_{11}+\mathrm{i}\lambda^*_{21})G_1+(\lambda^*_{12}+\mathrm{i}\lambda^*_{22})G_2,$$

the formula Eq. (37) provides evaluation of the effective conductivity tensor $\mathbf{\Lambda}^*$.

5. Numerical study

The model we have developed involves a number of parameters contributing to the effective conductivity of composite. They are volume content c of inclusions, their arrangement (Z_q), size and shape (l_1 and l_2), inclusion-to-matrix conductivity ratio $\tilde{\lambda}_1$ and normalized interface conductivity, $\tilde{h}_c$. In this numerical study, we keep $l_1=1$ and $\lambda_0=1$ fixed. Also, we limit our consideration by two model geometries of composite. One of them is a periodic orthogonal array whose periods a_1 and a_2 are proportional to inclusion's semi axes: $l_1/a_1=l_2/a_2$. Another one is the quasi-random geometry shown in Fig. 2, with $N=48$. Noteworthy, the last model can be also used to study the periodic structures provided the ratio a_1/a_2 is a rational number, see Figs. 3 and 4 for example. An alternate approach consists in considering the rectangle with sides a_1 and a_2 containing one inclusion as a unit cell of periodic composite. All the above theory, with appropriate modification of the standard lattice sums Σ^*_n Eq. (C.7), applies to this model as well.

The multiple inclusion model boundary-value problem reduces to an infinite linear system even in the case of perfect interface. Therefore, an accuracy of numerical (approximate, in fact) solution will depend on the number $n_{\max}$ of equations retained in Eq. (28). Some idea of the reported below numerical data can be drawn from Table 2, where the effective conductivity λ^*_{22} of periodic composite is shown as a function of $n_{\max}$ for volume content $c=0.7$

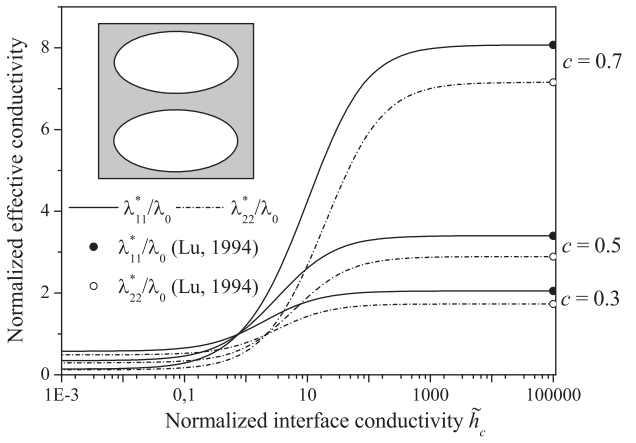

Fig. 3. Effective conductivities λ^*_{11} and λ^*_{22} of periodic composite with perfectly conducting inclusions ($\tilde{\lambda}_1 = \infty$) as a function of interface conductivity $\tilde{h}_c$: aspect ratio $e = 0.5$; volume content of inclusions $c = 0.3,\ 0.5$ and 0.7.

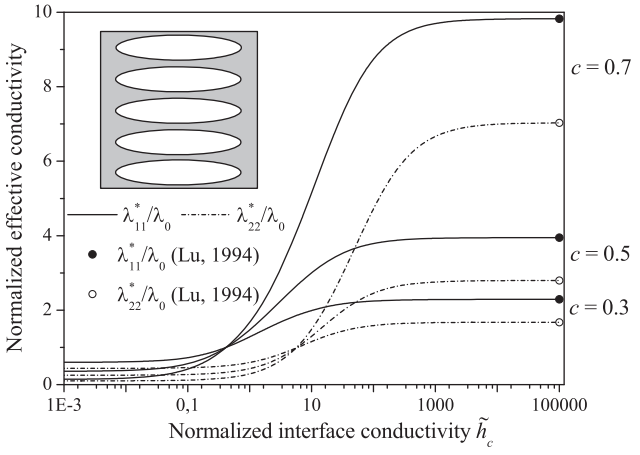

Fig. 4. Effective conductivities λ^*_{11} and λ^*_{22} of composite of perfectly conducting inclusions ($\tilde{\lambda}_1 = \infty$) as a function of interface conductivity $\tilde{h}_c$: aspect ratio $e = 0.2$; volume fraction of inclusions $c = 0.3,\ 0.5$ and 0.7.

and $\tilde{\lambda}_1 = 1000$. As seen from the table, the convergence rate is governed primarily by the volume content of inclusions or, what is the same, by the minimum distance between them. With $n_{\max}$ increased, the numbers computed from Eq. (37) converge to those obtained independently by solving the unit cell problem by the finite element method and shown in the bottom row of Table 2. It is seen from the table that for $c = 0.7 \approx 0.9c_{\max}$, where $c_{\max} = \pi/4$ corresponds to dense packing, $n_{\max} = 20$ provides evaluation of the effective conductivity of composite with at least 5-digit accuracy. What is important in the context of our study, λ^* convergence rate is practically invariant of h_c.

Table 2
Convergence rate of λ^*_{22}/λ_0 as a function of $n_{\max}$ for volume content $c = 0.7$ and conductivity ratio $\tilde{\lambda}_1 = 1000$.

$n_{\max}$	$e = 0.5$			$e = 0.2$		
	$\tilde{h}_c = 0$	$\tilde{h}_c = 10$	$\tilde{h}_c = \infty$	$\tilde{h}_c = 0$	$\tilde{h}_c = 10$	$\tilde{h}_c = \infty$
1	0.15696	2.49917	5.10142	0.13860	1.38832	4.71613
3	0.12590	2.64753	6.66346	0.10420	1.45461	6.37850
5	0.12428	2.65092	6.98261	0.10178	1.45310	6.82303
10	0.12396	2.65141	7.08665	0.10175	1.45340	6.95565
15	0.12394	2.65141	7.09175	0.10174	1.45342	6.96353
20	0.12394	2.65141	7.09181	0.10174	1.45342	6.96363
FEA	0.12394	2.6514	7.0918	0.1017	1.4534	6.9637

In Figs. 3 and 4, the components λ^*_{11} and λ^*_{22} of the effective conductivity tensor of periodic composite are plotted as a function of $\tilde{h}_c$. The perfectly conducting inclusions ($\tilde{\lambda}_1 = \infty$) with aspect ratio $e = 0.5$ (Fig. 3) and $e = 0.2$ (Fig. 4) are considered; their volume content $c = 0.3, 0.5$ and 0.7. Our computations show that for $\tilde{h}_c \geqslant 100$ the macroscopic conductivity is close to that of composite with perfect interface ($h_c = \infty$). In this limiting case, our results expectedly coincide with the accurate data by Lu (1994) shown by the solid and open circles. This can be regarded as a validation of both the theory and numerical algorithm of our method. For $\tilde{h}_c \leqslant 0.1$, conductivity of composite is close to that of porous solid – despite the fact that the conductivity of inclusions is infinitely large. This example clearly shows that an interface may affect overall conductivity of composite quite substantially and therefore should be taken into account.

Tables 3 and 4 contain the computed effective conductivity λ^*_{11} and λ^*_{22}, respectively, of periodic composite as a function of volume fraction, $\tilde{\lambda}_1$ and $\tilde{h}_c$. The aspect ratio of inclusions $e = 1/3$. Again, we observe substantial effect of interface conductivity on the macroscopic response of composite.

For $c = 0.5,\ \tilde{\lambda}_1 = 10$ and $h_c = \infty$, these data are consistent with those reported by Byström (2003), for $\tilde{\lambda}_1 = 1000$ and $h_c = \infty$ (perfect thermal contact) they agree with the results by Lu (1994).

Now, we proceed to composite of random structure. The below data were obtained from the RUC model (Fig. 2) containing $N = 48$ equally oriented ellipses. This model in the particular case of circular inclusions perfectly bonded to the matrix was studied by several authors (Kim and Torquato, 1990; Cheng and Greengard, 1997; Byström, 2003 among others), and so we start from comparison. In Table 5, an effective conductivity $\lambda^*_{11} = \lambda^*_{22}$ of composite with randomly placed circular ($e = 1$), perfectly conducting inclusions is shown as a function of their volume content c and normalized interface conductivity $\tilde{h}_c$. The last four columns of this table contain the data obtained by other authors for composite with perfect interface. They are labelled as follows: [C&G] – Cheng and Greengard (1997), [B] – Byström (2003), [M] – Milton (1981) and [K&T] – Kim and Torquato (1990). As comparison shows, our data for two limiting cases ($h_c = \infty$ and $h_c = 0$) are consistent with

Table 3
Effective conductivity λ^*_{11} of periodic composite as a function of volume content c, conductivity ratio $\tilde{\lambda}_1$ and normalized interface conductivity $\tilde{h}_c$.

c	$\tilde{\lambda}_1 = 1$			$\tilde{\lambda}_1 = 10$			$\tilde{\lambda}_1 = 1000$		
	$\tilde{h}_c = 0$	$\tilde{h}_c = 10$	$\tilde{h}_c = \infty$	$\tilde{h}_c = 0$	$\tilde{h}_c = 10$	$\tilde{h}_c = \infty$	$\tilde{h}_c = 0$	$\tilde{h}_c = 10$	$\tilde{h}_c = \infty$
0.1	0.8611	0.9937	1.0	0.8611	1.2084	1.2559	0.8611	1.2836	1.3564
0.2	0.7213	0.9874	1.0	0.7213	1.4148	1.5144	0.7213	1.5641	1.7189
0.3	0.5890	0.9812	1.0	0.5890	1.6409	1.8110	0.5890	1.8825	2.1595
0.4	0.4661	0.9749	1.0	0.4661	1.9021	2.1753	0.4661	2.2715	2.7509
0.5	0.3528	0.9688	1.0	0.3528	2.2165	2.6500	0.3528	2.7762	3.6256
0.6	0.2466	0.9626	1.0	0.2466	2.6107	3.3155	0.2466	3.4769	5.1175
0.7	0.1412	0.9566	1.0	0.1412	3.1321	4.3849	0.1412	4.5514	8.6142

Table 4
Effective conductivity λ_{22}^* of periodic composite as a function of volume content c, conductivity ratio $\widetilde{\lambda}_1$ and normalized interface conductivity $\widetilde{h}_c$.

c	$\widetilde{\lambda}_1 = 1$			$\widetilde{\lambda}_1 = 10$			$\widetilde{\lambda}_1 = 1000$		
	$\widetilde{h}_c = 0$	$\widetilde{h}_c = 10$	$\widetilde{h}_c = \infty$	$\widetilde{h}_c = 0$	$\widetilde{h}_c = 10$	$\widetilde{h}_c = \infty$	$\widetilde{h}_c = 0$	$\widetilde{h}_c = 10$	$\widetilde{h}_c = \infty$
0.1	0.7366	0.9687	1.0	0.7366	1.0692	1.1368	0.7366	1.0859	1.1611
0.2	0.5809	0.9391	1.0	0.5809	1.1496	1.3177	0.5809	1.1894	1.3853
0.3	0.4621	0.9108	1.0	0.4621	1.2413	1.5533	0.4621	1.3114	1.6962
0.4	0.3626	0.8834	1.0	0.3626	1.3451	1.8641	0.3626	1.4545	2.1419
0.5	0.2747	0.8567	1.0	0.2747	1.4622	2.2866	0.2747	1.6227	2.8276
0.6	0.1944	0.8307	1.0	0.1944	1.5942	2.8926	0.1944	1.8212	4.0373
0.7	0.1149	0.8048	1.0	0.1149	1.7433	3.8503	0.1149	2.0574	7.0149

Table 5
Effective conductivity $\lambda_{11}^* = \lambda_{22}^*$ of composite with randomly placed circular ($e = 1$), perfectly conducting inclusions as a function of volume content c and interface conductivity $\widetilde{h}_c$.

c	Eq. (37)				[C&G]	[B]	[M]	[K&T]
	$\widetilde{h}_c = 0$	$\widetilde{h}_c = 1$	$\widetilde{h}_c = 5$	$\widetilde{h}_c = \infty$				
0.1	0.813	0.991	1.115	1.182	1.182	1.182	1.182	–
0.2	0.651	0.981	1.246	1.410	1.410	1.410	1.408	1.41
0.3	0.508	0.972	1.393	1.698	1.698	1.697	1.690	–
0.4	0.388	0.963	1.56	2.07	2.067	2.068	2.049	2.07
0.5	0.285	0.953	1.75	2.55	2.546	2.543	2.512	–
0.6	0.200	0.944	1.98	3.18	3.186	3.170	3.123	3.14
0.7	0.131	0.935	2.23	4.00	4.020	3.945	3.927	–

those available in literature. To our best knowledge, only the approximate results are available in literature Lu and Song (1996) for the random structure composite with a finite h_c.

The paper by Byström (2003) is probably the only work where the RUC model of elliptic fiber composite with perfect interface was studied. The effective conductivity of composite containing elliptic inclusions with imperfect interface never been considered even approximately. The derived by us complete solution of this problem enables obtaining the reliable data for the random composite with elliptic fibers, imperfectly bonded to the matrix. The concentration dependencies $\lambda_{11}^*(c)$ and $\lambda_{22}^*(c)$ for a composite with $e = 1/3$ and $\widetilde{\lambda}_1 = 10$ are shown in Figs. 5 and 6, respectively. There, the curves 1–4 correspond to $\widetilde{h}_c = 0,\ 1,\ 5$ and ∞. Again, our results for $h_c = \infty$ are consistent with the data reported by Byström (2003) shown by the open circles in Figs. 5 and 6. The numerical data for a finite h_c have been obtained for the first time.

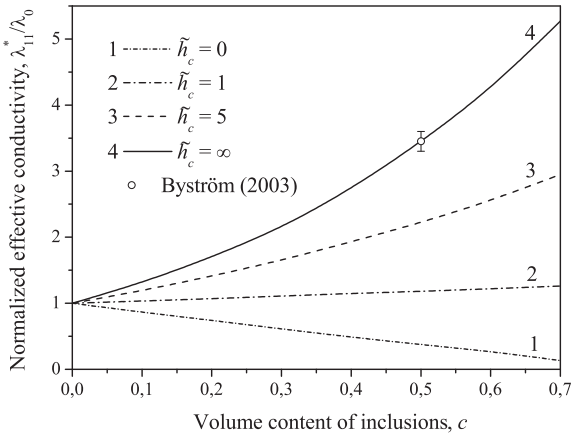

Fig. 5. Effective conductivity λ_{11}^* of random structure composite of elliptic ($e = 1/3$) inclusions as a function of volume content of inclusions c: bulk conductivity ratio $\widetilde{\lambda}_1 = 10$; normalized interface conductivity $\widetilde{h}_c = 0,\ 1,\ 5$ and ∞.

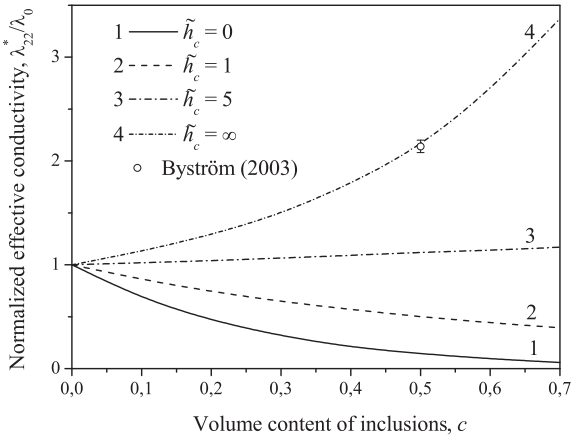

Fig. 6. Effective conductivity λ_{22}^* of random structure composite of elliptic ($e = 1/3$) inclusions as a function of volume content of inclusions c: bulk conductivity ratio $\widetilde{\lambda}_1 = 10$; normalized interface conductivity $\widetilde{h}_c = 0, 1, 5$ and ∞.

6. Conclusions

The interfaces greatly contribute to the local and overall behavior of heterogeneous solids and so should be taken into account adequately in the predictive models. Only one example is the Kapitza resistance which greatly reduces the thermal conductivity of composite at micro scale (e.g., Every et al., 1992). The problems involving composites with imperfect interface have received a considerable attention in the literature. However, the most work in the area is done for composites with spherical or circular inclusions. The micromechanical models able to predict the cumulative effect of interface shape and imperfectness degree on the composite's local and overall behavior are virtually absent in the literature. To address this problem, the analytical, Rayleigh type method has been developed to study the transverse conductivity and longitudinal shear of composite with the aligned elliptic fibers imperfectly bonded to the matrix. The complete, multipole expansion solution has been obtained for the local fields and effective properties of composite. Both the periodic and random microstructure of composite are considered. In the latter case, the representative unit cell of a composite contains multiple elliptic inclusions. Taking their number sufficiently large enables study the relationships between the micro structure statistics and macroscopic behavior of composite. The method combines the principle of superposition, technique of complex potentials and some new results in the theory of special functions. An appropriate choice of complex potentials and the re-expansion formulas for them reduce the boundary-value problem for a heterogeneous solid to an ordinary, well-posed set of linear algebraic equations. This in turn reduces the computational effort of solution and thus provides high numerical efficiency of the developed method. The exact, finite form expressions for the effective conductivity tensor have been derived by analytical averaging of the local temperature gradient and heat flux fields. The obtained

solution has been tested numerically for convergence and verified by comparison with the available numerical data for the particular cases. The accurate numerical data reported in the paper show a substantial effect of interface resistance on the effective conductivity of composite and can serve as a benchmark for the newly developed theories of composites with imperfect interface. Noteworthy, the assumption of aligned inclusions was made only for the simplicity sake and is in no way limiting. The developed theory applies equally to the multiphase and polydisperse composites with randomly placed and oriented elliptic inclusions with homogeneous interface resistance. Its extension to the composites with *inhomogeneously* imperfect interface (Ru and Schiavone, 1997) is straightforward. Yet another promising application of the developed theory is the nanocomposites with coherent interfaces (Luo and Wang, 2009). These problems will be addressed in the subsequent publications.

Acknowledgment

The authors gratefully acknowledge the support from the FP7 IRSES project TAMER IRSES-GA-2013-610547.

Appendix A. Evaluation of β_k coefficients

We re-write Eq. (18) as

$$\beta_k = -\frac{1}{2\pi}\frac{\lambda_1}{hl_2}\int_0^{2\pi}\frac{\cos k\eta - \mathrm{i}\sin k\eta}{\Delta(\alpha)}\mathrm{d}\eta,$$

where $\Delta(\alpha)=\sqrt{1+\alpha\sin^2\eta}$. It is readily seen that for all integer k

$$\int_0^{2\pi}\frac{\sin k\eta}{\Delta(\alpha)}\mathrm{d}\eta\equiv 0;\quad \int_0^{2\pi}\frac{\cos(2k+1)\eta}{\Delta(\alpha)}\mathrm{d}\eta\equiv 0;$$

so we only need to evaluate the integrals of type

$$I_k=\int_0^{2\pi}\frac{\cos 2k\eta}{\Delta(\alpha)}\mathrm{d}\eta=4\int_0^{\pi/2}\frac{\cos 2k\eta}{\Delta(\alpha)}\mathrm{d}\eta. \tag{A.1}$$

For $k=0$ and $k=1$, these integrals are written in terms of complete elliptic integrals of the first and second kind, defined as (Abramovitz and Stegun, 1964)

$$\mathrm{K}(\alpha)=\int_0^{\pi/2}\frac{\mathrm{d}x}{\Delta(-\alpha)}\quad\text{and}\quad \mathrm{E}(\alpha)=\int_0^{\pi/2}\Delta(-\alpha)\mathrm{d}x,$$

respectively. By comparison with Eq. (A.1), one finds

$$I_0=4\sqrt{\alpha}\mathrm{K}(-\alpha) \tag{A.2}$$

and

$$I_1=4\sqrt{\alpha}\left[\left(1+\frac{2}{\alpha}\right)\mathrm{K}(-\alpha)-\frac{2}{a}\mathrm{E}(-\alpha)\right]. \tag{A.3}$$

Now, we derive the recurrent formula for $I_k,\ k\geqslant 2$. The standard trigonometry consideration yields

$$\frac{I_{k+1}}{\sqrt{\alpha}}=\int_0^{2\pi}\frac{\cos 2k\eta\cos 2\eta}{\Delta(\alpha)}\mathrm{d}\eta-\int_0^{2\pi}\frac{\sin 2k\eta\sin 2\eta}{\Delta(\alpha)}\mathrm{d}\eta \tag{A.4}$$

and

$$\int_0^{2\pi}\frac{\cos 2k\eta\cos 2\eta}{\Delta(\alpha)}\mathrm{d}\eta=\frac{I_{k+1}+I_{k-1}}{2\sqrt{\alpha}}.$$

Also, we apply the differentiation formulas

$$\frac{2}{a}\mathrm{d}\Delta(\alpha)=\frac{\sin 2\eta\mathrm{d}\eta}{\Delta(\alpha)};\quad \mathrm{d}\sin 2k\eta=2k\cos 2k\eta\mathrm{d}\eta$$

and integration by parts to transform the second integral in Eq. (A.4):

$$\begin{aligned}\int_0^{2\pi}\frac{\sin 2k\eta\sin 2\eta}{\Delta(\alpha)}\mathrm{d}\eta&=\frac{2}{\alpha}\int_0^{2\pi}\sin 2k\eta\,\mathrm{d}\Delta(\alpha)\\&=\frac{2}{\alpha}\left[\sin 2k\eta\,\mathrm{d}\Delta(\alpha)^{1/2}\Big|_0^{2\pi}-\int_0^{2\pi}\Delta(\alpha)\mathrm{d}\sin 2k\eta\right]\\&=-2k\left(\frac{2}{\alpha}+1\right)\frac{I_k}{\sqrt{\alpha}}+2k\int_0^{2\pi}\frac{\cos 2k\eta\cos 2\eta}{\Delta(\alpha)}\mathrm{d}\eta.\end{aligned}$$

By combining the above formulas, we obtain the recurrent formula

$$\left(\frac{1}{2}+k\right)I_{k+)}=\left(\frac{1}{2}-k\right)I_{k-1}+2k\left(\frac{2}{\alpha}+1\right)I_k. \tag{A.5}$$

Together with Eqs. (A.2) and (A.3), Eq. (A.5) provides an efficient evaluation of I_k and hence β_k coefficients of Eq. (18).

Appendix B. Re-expansion formulas for the elliptic solid harmonics

The series expansion of the pth inclusion-related irregular elliptic harmonics $(\upsilon_p)^{-n}$ $(n>0)$ in a vicinity of another, qth inclusion is given by the formula (Kushch et al., 2005)

$$\upsilon_p^{-n}=\sum_{m=0}^{\infty}\eta_{nm}^{pq}\left(\upsilon_q^m+\upsilon_q^{-m}\right)\quad(n\geqslant 1); \tag{B.1}$$

where the expansion coefficients $\eta_{nm}^{pq}=\eta_{nm}(Z_{pq},d_p,d_q)$ and $Z_{pq}=Z_q-Z_p$. For the arbitrarily located, equally oriented elliptic coordinate frames $O_px_{1p}x_{2p}$ and $O_qx_{1q}x_{2q}$ with the same semi-foci parameter $d_p=d_q=d$, Yardley et al., 1999 have suggested the formula

$$\eta_{nm}(Z_{pq})=\frac{1}{\pi}\int_0^{\pi}(\upsilon_p)^{-n}\Big|_{\zeta_q=0}\cos(m\eta_q)d\eta_p. \tag{B.2}$$

Computational effort of η_{nm} evaluation from (B.2) is quite considerable. An efficiency of numerical algorithm can be improved by using two series expansions of η_{nm} (Kushch et al., 2005). The first one is

$$\begin{aligned}\eta_{nm}(Z)=(-1)^m n\sum_{j=0}^{\infty}V^{-(n+m+2j)}\times\sum_{l=0}^{j}\frac{(-1)^{j-l}}{(j-l)!}\left(\frac{1}{2}\right)^{n+m+2l}\\\times M_{nml}\frac{(n+m+l+j-1)!}{(j-l)!},\end{aligned} \tag{B.3}$$

where V is defined by $Z=d\left(V+V^{-1}\right)$. Here,

$$M_{nml}=\frac{(n+m+l+1)_l}{l!(n+l)!(m+l)!},$$

where $(n)_m$ is the Pohgammer's symbol. The series Eq. (B.1) with the coefficients Eq. (B.3) converges within an ellipse centered in Z_q with inter-foci distance $2d$ and passing the pole of pth elliptic coordinate frame closest to Z_q which is sufficient to solve for any two non-overlapping ellipses. For the well-separated (namely, $|z_p|>d,\ |z_q|<|Z_{pq}|$ and $|Z_{pq}|>2d$) inclusions, Eq. (B.3) simplifies to

$$\eta_{nm}(Z)=n(-1)^m\sum_{l=0}^{\infty}d^{2l+n+m}M_{nml}\frac{\Gamma(n+m+2l)}{(2Z)^{n+m+2l}}. \tag{B.4}$$

Appendix C. Periodic complex potentials

Following Kushch et al. (2009b), we define the functions $\widehat{\upsilon}_n$ as 2D lattice sums:

$$\widehat{\upsilon}_n(z)=\sum_{\mathbf{k}}[\upsilon(z+W_{\mathbf{k}})]^{-n}\quad(n\geqslant 1), \tag{C.1}$$

where $W_{\mathbf{k}}=a\mathbf{k}=a(k_1+\mathrm{i}k_2),\ -\infty<k_1,k_2<\infty$. The drawback of this definition is the convergence issue: in fact, the series Eq. (C.1) for $n=1$ is conditionally convergent (Kushch, 2013). An alternate

way of defining the functions $\widehat{\upsilon}_n$ uses their local series expansion of the form

$$\widehat{\upsilon}_n = \upsilon^{-n} + \sum_k \widetilde{\eta}_{nk}(\mathbf{0})(\upsilon)^{-k}, \tag{C.2}$$

where

$$\widetilde{\eta}_{nk}(z) = \sum_{\mathbf{k}\neq\mathbf{0}} \eta_{nm}(z + W_{\mathbf{k}}), \tag{C.3}$$

η_{nm} being the re-expansion coefficient defined by Eq. (B.1). For $n > 1$, the definitions by Eqs. (C.1) and (C.2) are equivalent. The periodic harmonics introduced this way obey the following periodicity conditions:

$$\widehat{\upsilon}_n(z + a) - \widehat{\upsilon}_n(z) = 0; \tag{C.4}$$

$$\widehat{\upsilon}_n(z + \mathrm{i}a) - \widehat{\upsilon}_n(z) = \delta_{n1}\frac{\pi d\mathrm{i}}{a}$$

and possess a countable set of cuts centered in the points $W_{\mathbf{k}}$. The series Eq. (C.1) is term wise differentiable; hence $\widehat{\upsilon}_n$ obeys Laplace equation and can be thought as the periodic complex potential.

In order to fulfil the boundary conditions at the qth inclusion, we need the local expansion of $\widehat{\upsilon}_n(z_p)$ in terms of υ_q. This regular expansion is readily derived with aid of the re-expansion formulas Eq. (B.1). We write it in the following form

$$\widehat{\upsilon}_n(z_p) = \sum_m \left(\eta_{nm}^{pq} + \widetilde{\eta}_{nm}^{pq}\right)(\upsilon_q)^{-m}, \tag{C.5}$$

where $\widetilde{\eta}_{nm}^{pq} = \widetilde{\eta}_{nk}(Z_{pq})$ and $\widetilde{\eta}_{nm}^{pq} = \widetilde{\eta}_{nk}(Z_{pq})$. In Eq. (C.5), Z_{pq} is understood as a minimum distance between the p-th and q-th inclusions, with account for those belonging to the adjacent cells: $Z_{pq} = \min(Z_q - Z_p \pm a \pm \mathrm{i}a)$. Then, the first term in Eq. (C.5) is computed using Eq. (B.3). As to the second one, given by Eq. (C.6), we note that $a \gg d$ for the typical RUC model. Therefore, Eq. (B.4) applies here and so we get

$$\widetilde{\eta}_{nm}^{pq} = n(-1)^m \sum_{l=0}^{\infty}\left(\frac{d}{2}\right)^{n+m+2l} M_{nml}\Gamma(n+m+2l)\Sigma^*_{n+m+2l}(Z_{pq}), \tag{C.6}$$

where Σ_n^* is the standard lattice sum defined as

$$\Sigma_n^*(z) = \sum_{\mathbf{k}\neq 0}(z + W_{\mathbf{k}})^{-n}. \tag{C.7}$$

References

Abramovitz, M., Stegun, I.A., 1964. Handbook for Mathematical Functions. NBS Applied Mathematics Series, vol. 55. Flammarion.

Achenbach, J.D., Zhu, H., 1989. Effect of interfacial zone on mechanical behaviour and failure of fibre-reinforced composites. J. Mech. Phys. Solids 37, 381–393.

Benveniste, Y., Miloh, T., 1986. The effective conductivity of composites with imperfect thermal contact at constituent interfaces. Int. J. Eng. Sci. 24, 1537–1552.

Byström, J., 2003. Influence of the inclusions distribution on the effective properties of heterogeneous media. Compos. Part B 34, 587–592.

Cheng, H., Greengard, L., 1997. On the numerical evaluation of electrostatic fields in dense random dispersions of cylinders. J. Comput. Phys. 136, 629–639.

Cheng, H., Torquato, S., 1997. Effective conductivity of periodic arrays of spheres with interfacial resistance. Proc. R. Soc. Lond. A 453, 145–161.

Cheng, H., Torquato, S., 1997. Effective conductivity of dispersions of spheres with a superconducting interface. Proc. R. Soc. Lond. A 453, 1331–1344.

Gao, J., 1995. A circular inclusion with imperfect interface: Eshelby s tensor and related problems. J. Appl. Mech. 62, 860–866.

Graham, S., McDowell, D.L., 2003. Numerical analysis of the transverse thermal conductivity of composites with imperfect interfaces. J. Heat Transfer 125, 389–393.

Hasselman, D.P.H., Johnson, L.F., 1987. Effective thermal conductivity of composites with interfacial thermal barrier resistance. J. Comput. Mater. 21, 508–515.

Every, A.G., Tzou, Y., Hasselman, D.P.H., Raj, R., 1992. The effect of particle size on the thermal conductivity of ZnS/diamond composites. Acta Metall. Mater. 40, 123–129.

Hashin, Z., 1990. Thermoelastic properties of fiber composites with imperfect interface. Mech. Mater. 8, 333–348.

Kantorovich, L.V., Krylov, V.I., 1964. Approximate Methods of Higher Analysis. Wiley, New York.

Kim, I.C., Torquato, S., 1990. Determination of the effective conductivity of heterogeneous media by Brownian motion simulation. J. Appl. Phys. 68, 3892–3903.

Kuo, H.-Y., 2010. Electrostatic interactions of arbitrarily dispersed multicoated elliptic cylinders. Int. J. Eng. Sci. 48, 370–382.

Kuo, H.-Y., 2013. Effective property of multiferroic fibrous composites with imperfect interfaces. Smart Mater. Struct. 22, 105005.

Kushch, V.I., Shmegera, S.V., Buryachenko, V.A., 2005. Interacting elliptic inclusions by the method of complex potentials. Int. J. Solids Struct. 42, 5491–5512.

Kushch, V.I., Shmegera, S.V., Buryachenko, V.A., 2006. Elastic equilibrium of a half plane containing a finite array of elliptic inclusions. Int. J. Solids Struct. 43, 3459–3483.

Kushch, V.I., Shmegera, S.V., Sevostianov, I., 2009a. SIF statistics in micro cracked solid: effect of crack density, orientation and clustering. Int. J. Eng. Sci. 47, 192–208.

Kushch, V.I., Sevostianov, I., Mishnaevsky Jr., L., 2009b. Effect of crack orientation statistics on effective stiffness of mircocracked solid. Int. J. Solids Struct. 46, 1574–1588.

Kushch, V.I., 2013. Micromechanics of Composites: Multipole Expansion Approach. Elsevier.

Kushch, V.I., Sevostianov, I., 2013. Dipole moments, property contribution tensors and effective conductivity of anisotropic particulate composites. Int. J. Eng. Sci. 74, 15–34.

Lu, S.-Y., 1994. Anisotropy in effective conductivities of rectangular arrays of elliptic cylinders. J. Appl. Phys. 76, 2641–2647.

Lu, S.-Y., Lin, H.-C., 1995. Effect of interfacial characteristics on effective conductivities of isotropic two-dimensional periodic composites. Chem. Eng. Sci. 50, 2611–2631.

Lu, S.-Y., Song, J.-L., 1996. Effect of interfacial characteristics on effective conductivities of composites containing randomly distributed aligned long fibers. Chem. Eng. Sci. 51, 4393–4404.

Luo, J., Wang, X., 2009. On the anti-plane shear of an elliptic nano inhomogeneity. Eur. J. Mech. A/Solids 28, 926–934.

Milton, G.W., 1981. Bounds on the transport and optical properties of a two-component composite material. J. Appl. Phys. 52, 5294–5304.

Muskhelishvili, N.I., 1953. Some Basic Problems of the Mathematical Theory of Elasticity. P. Noordhoff, Groningen.

Ru, C.Q., Schiavone, P., 1996. On the elliptic inclusion in anti-plane shear. Math. Mech. Solids 1, 327–333.

Ru, C.Q., Schiavone, P., 1997. A circular inclusion with circumferentially inhomogeneous interface in antiplane shear. Proc. R. Soc. Lond. Ser. A 453, 2551–2572.

Shen, H., Schiavone, P., Ru, C.Q., Mioduchowski, A., 2000. An elliptic inclusion with imperfect interface in anti-plane shear. Int. J. Solids Struct. 37, 4557–4575.

Sneddon, I.N., Berry, D.S., 1958. The Classical Theory of Elasticity. Springer.

Yardley, R.C., McPhedran, J.G., Nicorovici, N.A., 1999. Addition formulas and the Rayleigh identity for arrays of elliptical cylinders. Phys Rev. E 60, 6068–6080.

Yardley, J.G., Reuben, A.J., McPhedran, R.C., 2001. The transport properties of layers of elliptical cylinders. Proc. R. Soc. Lond. A 457, 395–423.

Zuzovsky, M., Brenner, H., 1977. Effective conductivities of composite materials composed of cubic arrangements of spherical particles embedded in an isotropic matrix. Z. Agnew. Math. Phys. (ZAMP) 28, 979–992.